Adaptive Regularization for Uniform Noise Covariance in Iterative 3D CT

Zhiqian Chang, Ruoqiao Zhang, Jean-Baptiste Thibault, Debashish Pal, Lin Fu, Ken Sauer, Charles Bouman

***Abstract*—Spatially varying noise behavior is problematic for many regularized statistical methods of reconstruction in X-ray CT. By adopting a very simple, approximate separation of the noise spectrum into low and high spatial frequencies, we arrive at a choice for adaptive regularization that appears to minimize variation in high-frequency noise character with dose, orientation and image content.**

I. INTRODUCTION

Model-based statistical methods of X-ray CT image reconstruction have shown promise in maintaining diagnostic image quality across a wider range of dosage than has been routinely practical [1], [2] with deterministic methods. The Bayesian (MAP) estimate is frequently formulated as

$$\hat{x} = \arg\min_{x \in \Omega} \left\{ \frac{1}{2}(y - Ax)^t W (y - Ax) + U(x) \right\}, \quad (1)$$

where W is a diagonal matrix with non-zero entries $\{w_j\}$, A is the modeled forward projection matrix, y is a set of integral projection measurements, and $U(x)$ is a function penalizing local voxel differences. This quadratic approximation to the log-likelihood has served well for a broad range of X-ray CT reconstruction tasks. The most crucial difference from traditional algebraic reconstruction techniques is the weighting matrix W, which may be viewed as an estimate of the inverse variance of each measurement. Entries in this matrix may vary by orders of magnitude in common CT applications, offering potential for greatly improved noise/resolution trade-offs. The Hessian of this formulation, $A^t W A$, is an approximation to the Fisher Information matrix for estimating voxel values from the sinogram data.

The quality of information available may vary widely across a CT reconstruction, as attenuation may reduce photon count levels by many orders of magnitude in dense materials or large patients. The MAP estimate will therefore smooth noise to varying degrees and with varying spatial correlation structure across the volume to be estimated. While this non-stationarity in noise may be an inherent feature of the optimal estimate in the sense in which we have formulated the problem, spatial uniformity of noise characteristics may be desirable in practice. Within the framework of the prior weighting for uniform resolution of Fessler and Rogers [3], we propose an alternative weighting option to achieve approximately uniform, rotationally-invariant noise covariance under full-coverage scans. Recent work by Cho and Fessler [4] proceeds from a set of assumptions different from ours and arrives at somewhat different results, but a similar modification of the weighting scheme from the uniform-resolution approach.

This work was supported by GE Healthcare.

Zhiqian Chang and Ken Sauer are with the Department of Electrical Engineering, University of Notre Dame, Notre Dame, IN 46556-5637.

Ruoqiao Zhang and Charles Bouman are with Department of Electrical and Computer Engineering, Purdue University, West Lafayette, IN 47907-0501

Jean-Baptiste Thibault and Debashish Pal are with Applied Science Laboratory, GE Healthcare, 3000 N. Grandview Blvd, Waukesha, WI 53188

Lin Fu is with the CT Systems and Applications Laboratory, GE Global Research, Niskayuna, NY 12309.

II. REGULARIZATION FOR NOISE UNIFORMITY

Some form of regularization is necessary in most CT applications and is especially critical in low signal settings. $U(x)$ can be chosen as a simple quadratic smoothing penalty, or a stochastic model including more flexibility in the sanction of image characteristics [5]. The majority of common models is described by

$$U(x) = \frac{1}{f(\zeta)} \sum_{(i,k) \in \mathcal{C}} b_{i,k} \rho(x_i - x_k) \quad (2)$$

with $\rho()$ a symmetric function of local pixel/voxel differences, $b_{i,k}$ weights according to relative location of neighbors, $\mathcal{C}$ is the collection of all pairs that contribute to the penalty, and $f()$ is a scaling related to the expectation of local image differences. Although numerous options for design of $\rho()$ are available in the literature, there are fewer available results and less consensus on the so-called "hyper-parameters" that control the balance between fidelity to data and faithfulness to *a priori* modeling. If a single parameter serves this function, it will be $f(\zeta)$ above, and the *a priori* image model is stationary, probably the most common assumption.

The Hessian of the log-likelihood, $A^t W A$, may have several orders of magnitude of dynamic range in its diagonal entries, due to proportional variation in the weighting matrix W. X-ray survival rates may range from 1 to 10^{-4} or less in common scans through dense tissue and large patients. The quality of data may also vary dramatically in the orientation of individual rays, causing oriented noise artifacts. All common Bayesian estimators adjust between adherence to prior modeling and fidelity to data as SNR varies. If we assume a stationary image model, with the scalar $f(\zeta)$ set heuristically to a good compromise between resolution and noise suppression, those two qualities may vary widely in their balance across an image.

In a clinical setting, consumers of reconstructed images may be less interested in achieving results that are optimal in a modeled statistical sense than in maintaining image attributes across widely varying signal-to-noise ratios (SNRs) typical of tomographic scans. Fessler and Rogers [3] provided a framework for spatially-adaptive control of the trade-off between

the two components of the objective with the modification of (2) to

$$\hat{U}(x) = \frac{1}{f(\zeta)} \sum_{(i,k)\in\mathcal{C}} b_{i,k}\hat{\kappa}_i\hat{\kappa}_k\rho(x_i - x_k), \tag{3}$$

where each $\hat{\kappa}_i$ is square-root of the i-th diagonal element of the approximate Fisher information matrix. The choice of inserting a data-dependent term into what is, in the Bayesian framework, considered the log of the *a priori* density runs counter to definitions of the objective's components, but is an effective adaptive component. In [3] the goal was approximately constant resolution in the image estimate in the face of widely varying pixel-wise Fisher information. We seek constant noise characteristics across the same variations.

For the sake of tractability, we begin with the case in which U is a quadratic function, or $U(x) = \frac{\zeta}{2}x^tRx$, with R having unity on the diagonal and negative values totaling unity in each set of off-diagonal row or column entries. This is the conventional Gaussian *a priori* image model with $f(\zeta) = \frac{2}{\zeta}$. We then arrive at the MAP estimator from (1) as a linear function of sinogram data:

$$\hat{x} = (A^tWA + \zeta R)^{-1}A^tWy.$$

Given that y contains additive zero-mean noise n in the sinogram vector, we may also write the image-domain error due to that noise as

$$\hat{e} = (A^tWA + \zeta R)^{-1}A^tWn.$$

The covariance of the noise in the reconstructed image has the form

$$\begin{aligned} E[\hat{e}\hat{e}^t] = \\ &(A^tWA + \zeta R)^{-1}A^tWE[nn^t]WA(A^tWA + \zeta R)^{-1} \\ &= (A^tWA + \zeta R)^{-1}A^t\tilde{W}A(A^tWA + \zeta R)^{-1}. \end{aligned} \tag{4}$$

The matrix $\tilde{W}$ is diagonal, having elements $w_j^2\xi_j^2$, with ξ_j^2 the Poisson/Gaussian signal dependent variance of the j-th sinogram entry. If we use conventional statistical weighting, $w_j \approx \xi_j^{-2}$ and $\tilde{w_j} \approx w_j$. A^tWA is low-frequency, approximated in the frequency domain by $1/||\omega||$ when W is constant on its diagonal and zero elsewhere. R is a high-frequency penalizing function and therefore will have its larger eigenvalues matched with high frequency eigenvectors. If we approximate the operator $(A^tWA + \zeta R)$ as having its eigenvalues separated between the first and second terms into components at low and high frequencies, we may rewrite (4) as

$$\begin{aligned} E[\hat{e}\hat{e}^t] \approx \\ &(A^tWA)^{-1}(A^t\tilde{W}A)(A^tWA)^{-1} + \zeta^{-2}R^{-1}A^t\tilde{W}AR^{-1} \end{aligned} \tag{5}$$

Each of these terms represents a "tail" of an operator away from its passband. Should we use weighting in the likelihood term with W as the approximate inverse covariance matrix of the data, $W \approx \tilde{W}$ and the first term is recognizable as the inverse of the Fischer information matrix, which would supply a lower bound on covariance for the ML estimator. Since the *a priori* density assigns little penalty to low frequencies, it is to be expected that the noise covariance would have the given form in this unregularized portion of the spectrum.

For visual quality of many CT images, the effects of noise having the greatest impact are those at higher spatial frequencies, and we consider the second term of (5). The penalty enforced by a conventional low-order Markov model described by R is high-frequency (for encouragment of low-pass behavior) which makes R^{-1} a low-pass operator. We approximate R^{-1} as constant in its stop-band. The second term of (5) then simplifies to

$$c_2\zeta^{-2}A^t\tilde{W}A,$$

an operator whose spatial characteristics are not difficult to visualize. The local covariance will have the familiar $1/|x|$ shape, but has strong tails in the direction of rays with large entries in $\tilde{W}$, corresponding to high count sinogram entries when W has detector photon counts on its diagonal. This long spatial correlation may be the statistical characterization of elevated probability of noise streaks in low-attenuation directions. Setting $w_j = \xi_j^{-1}$ restores isotropic covariance (under assumption of isotropic A^tA) by making $\tilde{W} = I$. In the X-ray CT problem, ξ_j^{-1} is approximated by $\sqrt{\lambda_j}$, where λ_j is the observed j-th photon count. This modification is a substantial change to the log-likelihood function, departing from the Poisson counting model but previously shown to offer advantages in some CT nondestructive testing applications [6].

We are interested particularly in the diagonal entries of $E[ee^t]$ for local noise variance. For the sake of our next approximate analysis, we let $\tilde{W} = W$ such that the first term of (5) reduces. We know from theory of positive definite matrices that

$$[(A^tWA)^{-1}]_{ii} \geq \frac{1}{(A^tWA)_{ii}}. \tag{6}$$

Since the spatial structure of the A matrix does not typically vary greatly over varying scans, we conjecture that (6) may, for local approximations, be made an equality with an appropriate scaling constant on one side. Let us furthermore approximate the low-pass filter R^{-1} as being flat across the high frequencies to which the second term in (5) corresponds, such that it may be replaced by a constant. The mean-squared noise error at voxel j may then be written as

$$E[\hat{e}_i^2] \approx \frac{c_1}{\sum_{j=1}^M w_iA_{ji}^2} + \frac{c_2\sum_{j=1}^M \tilde{w}_jA_{ji}^2}{\zeta^2} \tag{7}$$

This rough analysis tells us that, with ζ fixed, noise variance at low frequencies drops as the inverse of effective voxel dosage (EVD) (as measured by photon counts times sampling rates times projection weights squared), while high frequency noise variance rises proportionally to EVD.

Should we wish to maintain constant noise variance across EVDs, a starting point may be to ignore the low frequency noise components, and attempt to fix the second term in (7). Thus we may replace our current ζ with

$$\zeta_{EVD} = \zeta(\sum_{j=1}^M \tilde{w}_jA_{ji}^2)^{\frac{1}{2}}. \tag{8}$$

Maintaining the variables $\{\kappa_i\}$ as prior scaling as in [3], this would correspond to

$$\kappa_i = (\sum_{j=1}^{M} \tilde{w}_j A_{ji}^2)^{\frac{1}{4}}. \quad (9)$$

A result that is similar for the full-view case is derived by an alternative route in [4].

III. Results

We apply the proposed methods to helical CT scan data acquired on a Discovery CT750 HD scanner (GE Healthcare, Waukesha, WI), at X-ray tube voltage of 120 kVp. All data is composed of 984 views per rotation at pitch of 1.0, 1.0 sec/rotation and 20 mm collimation. As illustration of the effects of adaptive regularization with uniform noise levels as goal in Section II, we compare spatial noise variation of three *a priori* weighting schemes in scans of a human torso phantom, with modest tube current of 25mA. This places our data in the lower end of practical dosage range, in keeping with the theme of this paper. Additionally, a second dosage level of 200mA shows the behavior of the method under varying global signal-to-noise levels.

The first of the models is the standard penalty of (2), in which the regularizing prior term is spatially invariant. This allows the balance between the log-likelihood and prior term to vary according to local Fisher information, with lower dosage areas, featuring greater uncertainty, being smoothed more severely. The second is the adaptive weighting of (3), intended to maintain nearly constant resolution while allowing noise variance to respond accordingly, becoming more prominent in low-count areas. Finally, we add our proposed modification of (9) in the hope of maintaining noise levels which vary little over both spatial displacement and overall dosage. The strength of regularization for each technique is adjusted manually to yield approximately equal noise levels among the methods in soft tissues near the surface of the abdomen at 25mA.

Not surprisingly, since the proposed model is designed for the sake of noise uniformity, it shows superior noise control in this sense. In Figure 1, we compare axial images from abdomen area, where the data-independent prior scaling produces over-smoothed texture at image central region, while the constant resolution kappa scaling leaves central region under-regularized. The proposed method generates an image with far less spatial variation in noise levels. Measured means and standard deviations in selected ROI's are shown in Table I. Figure 2 shows coronal images, of the phantom. With data-independent prior scaling, we again see that the region with lower counts is generally over-regularized, with attendant loss of spatial resolution. In contrast, the constant resolution kappa appears to under-regularize the low-counts area. Some anatomical structures are compromised in the consequently higher noise. In Figure 2a, abdominal tissues near the spine are over-smoothed, and some high frequency information is attenuated, and the variance in cardiac tissue is significantly higher than in any other region. Figure 2b shows the opposite situation, where the standard deviation in central abdominal region can be as high as triple that of cardiac tissue. The proposed prior scaling method again achieves a more spatially consistent balance between image spatial resolution and noise suppression. The noise strength throughout the body volume manages to stay relatively constant, shown in Figure 2c. In practice, this would appear to serve better for diagnostic purposes.

Raising the tube current to 200mA reduces sinogram data variance by a factor of approximately 8 and would therefore be expected to reduce image noise standard deviation by approximately 2.8 in conventional reconstruction methods. Regularizing for constant resolution will amplify the difference yet more strongly. Our uniform noise approach limits the noise deviation reduction to a factor of about 1.5 between the two dosage levels, and channels the improved SNR primarily into resolution improvement at higher dosage, as illustrated in image (d) of Figures 1-2 and Tables I-II.

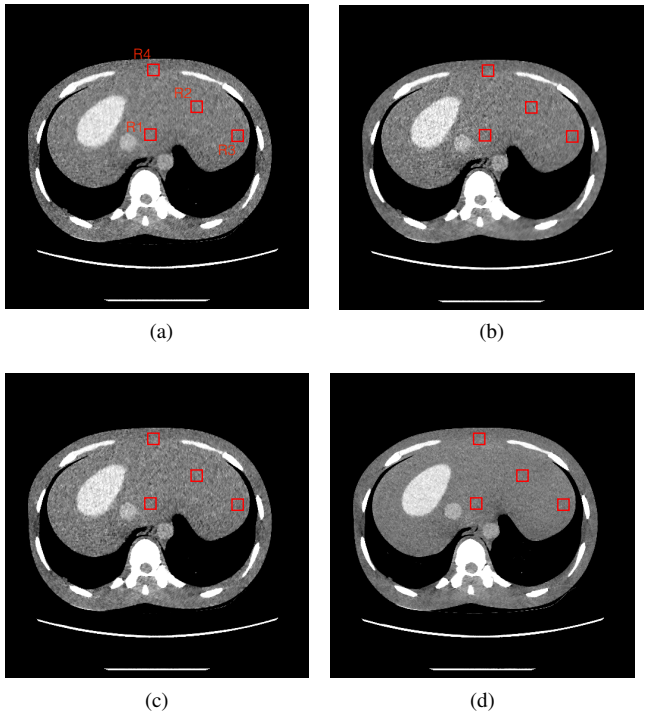

(a) (b) (c) (d)

Fig. 1: Torso axial images at abdomen region. (a): data-independent prior scaling at 25mA; (b): constant resolution κ_i at 25mA; (c): constant noise κ_i at 25mA; (d): constant noise κ_i at 200mA. Window width 200 HU.

IV. Conclusion

Our approach to uniform noise rendering yields relatively robust control of noise levels consistent across spatially varying X-ray penetration and overall dosage adjustments. Such uniformity would appear preferable to radiologists for diagnostic purposes. Our subsequent work with these innovations will include clinical applications and more extensive, quantitative phantom studies.

TABLE I: Noise measurements (means and standard deviations) at selected ROI's in torso axial images (HU).

	ROI 1	ROI 2	ROI 3	ROI 4	
data-independent prior	-2.05	-1.79	-6.42	-3.65	mean
(120kV, 25mA)	8.50	10.85	12.63	12.24	std
constant resolution kappa	-2.87	-2.49	-6.33	-3.99	mean
(120kV, 25mA)	15.16	11.93	8.16	11.86	std
constant noise kappa	-2.73	-2.21	-6.28	-3.87	mean
(120kV, 25mA)	13.51	13.46	12.49	13.33	std
constant noise kappa	-2.81	-3.29	-5.35	-4.51	mean
(120kV, 200mA)	10.98	9.69	9.11	9.99	std

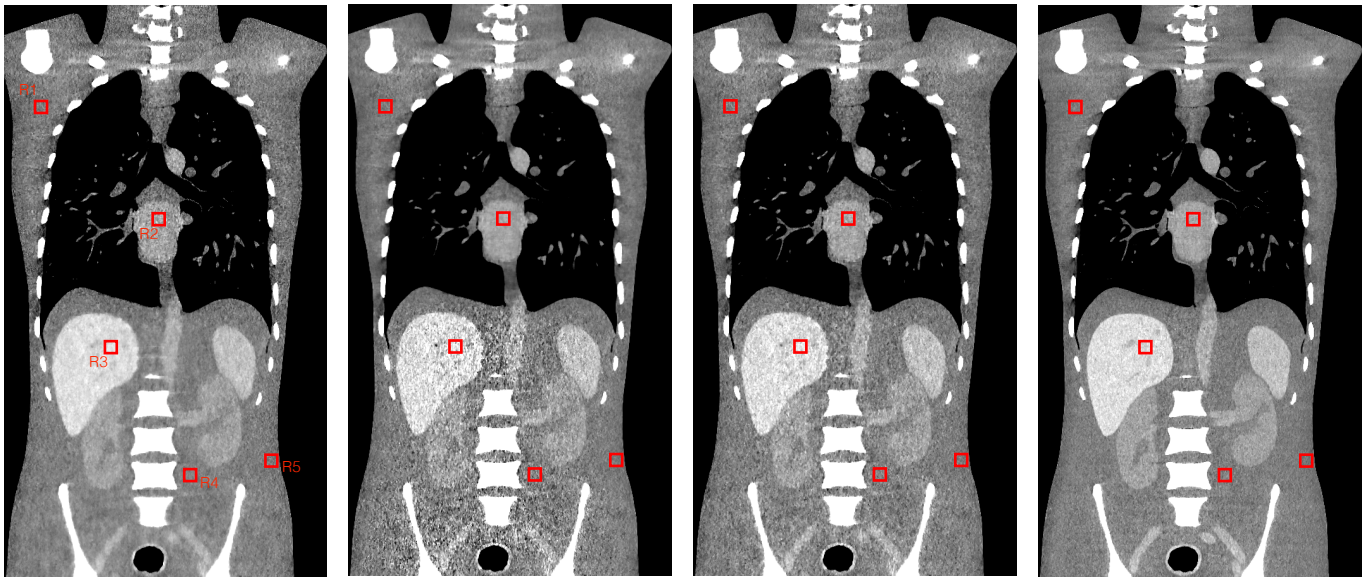

(a) (b) (c) (d)

Fig. 2: Torso coronal images. (a): data-independent prior scaling at 25mA; (b): constant resolution κ_i at 25mA; (c): constant noise κ_i at 25mA; (d): constant noise κ_i at 200mA. Window width 200 HU.

TABLE II: Noise measurements (means and standard deviations) at selected ROI's in torso coronal images (HU).

	ROI 1	ROI 2	ROI 3	ROI 4	ROI 5	
data-independent prior	-2.33	32.15	76.08	3.48	-3.60	mean
(120kV, 25mA)	12.36	17.10	7.56	6.52	14.24	std
constant resolution kappa	-3.35	32.06	76.45	4.71	-5.24	mean
(120kV, 25mA)	8.78	7.06	30.99	19.92	9.33	std
constant noise kappa	-2.63	31.81	76.96	4.20	-3.58	mean
(120kV, 25mA)	12.69	12.21	15.93	13.41	13.37	std
constant noise kappa	-3.24	30.69	70.31	1.34	-7.77	mean
(120kV, 200mA)	8.25	9.08	11.10	11.43	7.95	std

REFERENCES

[1] J.-B. Thibault, K. Sauer, C. Bouman, and J. Hsieh, "A three-dimensional statistical approach to improved image quality for multi-slice helical CT," *Medical Physics* **34**, pp. 4526–4544, November 2007.

[2] A. Ziegler, T. Köhler, and R. Proksa, "Noise and resolution in images reconstructed with FBP and OSC algorithms for CT," *Medical Physics* **34**, pp. 585–598, February 2007.

[3] J. Fessler and W. L. Rogers, "Spatial resolution properties of penalized-likelihood image reconstruction methods: Space-invariant tomographs," *IEEE Trans. on Image Processing* **5**, pp. 1346–1358, September 1996.

[4] J. H. Cho and J. A. Fessler, "Regularization designs for uniform spatial resolution and noise properties in statistical image reconstruction for 3D X-ray CT," *IEEE Trans. on Medical Imaging* **34**, pp. 678–689, February 2015.

[5] S. Z. Li, *Markov Random Field Modeling in Image Analysis*, Springer Science and Business Media, 2009.

[6] J. Kisner, P. Jin, C. Bouman, and K. Sauer, "Model refinement for a helical CT security baggage scanner," in *Proc. of 47th IEEE Carnahan Conf. on Security Technology*, (Medillín, Colombia), 2013.